TOTEM PHYSICS

G. Anelli[1], A. Aurola[2], V. Avati[1], V. Berardi[3], U. Bottigli[4], M. Bozzo[5], E. Brücken[2], A. Buzzo[5], M. Calicchio[3], F. Capurro[5], M.G. Catanesi[3], M.A. Ciocci[4], S. Cuneo[5], C. Da Già[6], M. Deile[1], E. Dimovasili[1], K. Eggert[1], M. Eräluoto[2], F. Ferro[5], A. Giachero[5], J. Hasi[6], F. Haug[1], J. Heino[2], T. Hilden[2], P. Jarron[1], J. Kalliopuska[2], J. Kašpar[7], A. Kok[6], V. Kundrát[7], K. Kurvinen[2], S. Lami[4], J. Lämsä[2], G. Latino[4], R. Lauhakangas[2], E. Lippmaa[8], J. Lippmaa[2], M. Lokajíček[7], M. LoVetere[5], D. Macina[1], M. Macrí[5], M. Meucci[4], S. Minutoli[5], A. Morelli[5], P. Musico[5], M. Negri[5], H. Niewiadomski[1], E. Noschis[1], J. Ojala[2], F. Oljemark[2], R. Orava[2], M. Oriunno[1], K. Österberg[2], R. Paoletti[4], A.-L. Perrot[1], E. Radermacher[1], E. Radicioni[3], E. Robutti[5], L. Ropelewski[1], G. Ruggiero[1], A. Rummel[8], H. Saarikko[2], G. Sanguinetti[4], A. Santroni[5], S. Saramad[1], F. Sauli[1], A. Scribano[4], G. Sette[5], J. Smotlacha[7], W. Snoeys[1], C. Taylor[9], A. Toppinen[2], A. Trummal[8], N. Turini[4], N. Van Remortel[2], L. Verardo[5], A. Verdier[1], S. Watts[6], J. Whitmore[10]

[1]*CERN, Genève, Switzerland,*
[2]*Helsinki Institute of Physics and University of Helsinki, Finland,*
[3]*INFN Sezione di Bari and Politecnico di Bari, Bari, Italy,*
[4]*Università di Siena and Sezione INFN-Pisa, Italy,*
[5]*Università di Genova and Sezione INFN, Genova, Italy,*
[6]*Brunel University, Uxbridge, UK,*
[7]*Academy of Sciences of the Czech Republic and Institute of Physics, Praha, Czech Republic,*
[8]*National Institute of Chemical Physics and Biophysics NICPB, Tallinn, Estonia.*
[9]*Case Western Reserve University, Dept. of Physics, Cleveland, OH, USA,*
[10]*Penn State University, Dept. of Physics, University Park, PA, USA*

Presented by K. Eggert

This article discusses the physics programme of the TOTEM experiment at the LHC. A new special beam optics with $\beta^* = 90$ m, enabling the measurements of the total cross-section, elastic pp scattering and diffractive phenomena already at early LHC runs, is explained. For this and the various other TOTEM running scenarios, the acceptances of the leading proton detectors and of the forward tracking stations for some physics processes are described.

1   Introduction

The physics programme of the TOTEM experiment can be performed in several few-days runs per year with special optics during the first three years of the "Large Hadron collider" (LHC) operation. As stated in the Letter of Intent [1] and the Technical Design Report [2], the principal goals of TOTEM are:

- the measurement of the total cross-section with a precision of about $1\,\mathrm{mb}$ using, via the Optical Theorem, the luminosity independent method that requires the simultaneous measurements of the total inelastic rate and the elastic pp scattering down to four-momentum transfers $(-t \approx p^2\theta^2)$ of a few $10^{-3}\,\mathrm{GeV}^2$;

- the measurement of the elastic pp scattering over a wide range in $-t$, up to $10\,\mathrm{GeV}^2$; and

- the study of inelastic diffractive final states that will comprise almost a quarter of all interactions.

The TOTEM programme focuses on physics not available to the general purpose experiments at the LHC. The experimental set-up, as described in the TDR [2] and in these proceedings [3], has therefore to be capable of meeting the challenges of detecting inelastically produced particles in the very forward region as well as protons very close to the LHC beams. It is comprised of Roman Pot detectors for the leading proton measurement together with tracking stations T1 and T2 in the very forward region of CMS.
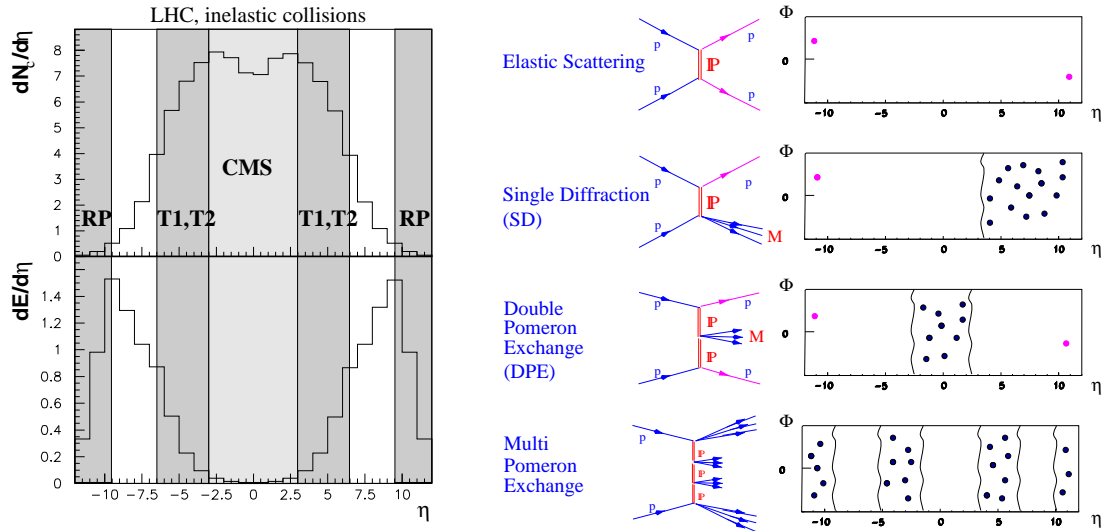

Figure 1: Left: pseudorapidity distribution of the charged particle multiplicity (upper part) and of the energy flow (lower part) per generic inelastic event; the grey bands correspond to the acceptance of the TOTEM detectors, while CMS covers the centre. Right: some diffractive process classes as Feynman diagrams, and their particle distributions in the rapidity-azimuth plane.

The combined CMS and TOTEM detectors cover an unprecedented pseudorapidity range for charged and neutral particles together with an excellent acceptance for leading protons. This is demonstrated in Fig. 1 (left) where the charged particle multiplicity and the energy flow in generic inelastic events is shown together with the common CMS/TOTEM acceptance. It is obvious that detectors like ATLAS and CMS, being optimised for hard QCD processes, will miss most of the energy. Never before has an experiment been constructed at a hadron collider with such a wide acceptance together with an excellent measurement of the leading protons. The large coverage of such a "combined experiment" will allow for unique measurements that will

be discussed in the near future in a common CMS/TOTEM physics report. The wide variety of diffractive processes that can be addressed is sketched in the rapidity-azimuth distributions (Fig. 1, right) taken from the FELIX proposal [4]. Starting with the cleanest process of elastic scattering up to the most complicated structure of multi-gap events due to multi-Pomeron exchange, diffraction can be precisely studied from soft to very hard processes, including high-p_T jets, heavy particles, W and Z, and possibly new particles, as discussed in Ref. [5]. As an example, Double Pomeron Exchange (DPE) offers the possibility of turning the LHC into an almost clean gluon factory, constrained by the measured momentum loss of the two forward protons. In this way, precise QCD studies and a search for new particles, created by gluon-gluon interactions, can be performed.

Furthermore, the observation of events over the full range of pseudorapidity can contribute significantly to cosmic-ray astrophysics and to the resolution of some of its outstanding problems [6]. It will open previously inaccessible regions of parameter space to quantitative studies where cosmic ray experiments have hinted at unusual physics.

2   Running Scenarios

2.1   Overview

The versatile programme of TOTEM requires different running scenarios that have to be adapted to the LHC commissioning in the first few years. A summary is given in Tab. 1.

Table 1:   TOTEM(+CMS) Diffractive Running Scenarios (k: number of bunches, N: number of protons per bunch)

Scen.	β^*[m]	k	$N/10^{11}$	$\mathcal{L}$[cm^{-2}s^{-1}]	$|t|$-range [GeV^2]	Objectives
1	1540	43	0.3	2×10^{28}	$0.002 \div 1.5$	low $|t|$ elastic, σ_T, min. bias, soft diffraction
2	1540	156	0.6÷1.15	2×10^{29}	$0.002 \div 1.5$	diffraction
3	90	156	1.15	3×10^{30}	$0.03 \div \sim 2$	intermediate $|t|$ elastic, σ_T
4	90	936	1.15	2×10^{31}	$0.03 \div \sim 2$	(semi-) hard diffraction
5	18	2808	1.15	3.6×10^{32}	$0.6 \div 8$	large $|t|$ elastic
6	0.5	2808	0.3	10^{33}	$1 \div \sim 10$	rare diffractive processes

Contrary to other detectors, the leading proton measurement critically depends on the focussing of the beams at the Intersection Point (IP), expressed by the betatron value (β^*). For the low-t measurements, the detection of protons with scattering angles of a few microradians requires the development of special beam optics with a β^* value as large as possible. The dedicated TOTEM optics with $\beta^* = 1540$ m are characterised by a small beam divergence ($0.3 \, \mu$rad) and by parallel-to-point focussing in both projections at the location of the Roman Pot detectors, 220 m away from the IP. As a consequence, the beam size at the IP is large, and at most 156 bunches are allowed in the machine to avoid parasitic bunch crossings, thus leading to low luminosities.

At the start of the LHC, the machine will be operated with only a few bunches and with a reduced proton density per bunch and zero degree crossing angle. The beams will then be gradually squeezed to β^* values around a few metres. TOTEM might request at that time a relaxation of the beams to $\beta^* = 90$ m for some few-days runs. This would make a measurement of elastic scattering with $-t$ values above $0.03 \, \text{GeV}^2$ possible and allow an early crude determination of the total cross-section. As discussed later, this optics scenario would also provide an excellent measurement of the momentum loss of diffractive protons, opening the studies of soft and semi-hard diffraction.

With the nominal optics ($\beta^* = 0.5\,\mathrm{m}$), TOTEM will register elastically scattered protons at large $|t|$ values and diffractive protons with a momentum loss above $2\,\%$. In this running condition, TOTEM and CMS together can study hard diffraction.
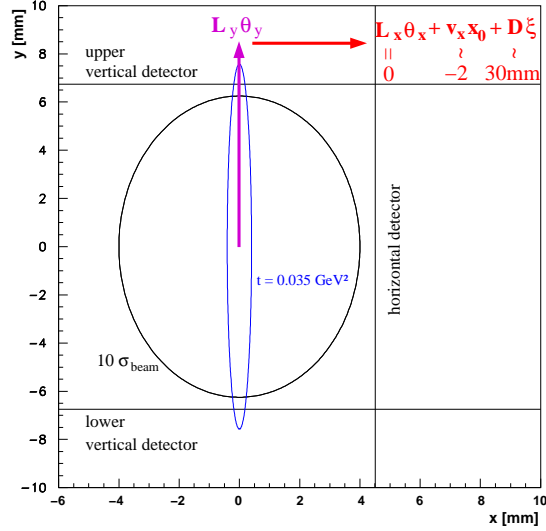
2.2 Optics with an Intermediate β^*

Figure 2: Principle of measuring the momentum loss ξ of diffractively scattered protons with the $\beta^* = 90\,\mathrm{m}$ optics. The large effective length L_y acts on the protons' vertical scattering angle θ_y to move them out of the beam, whereas the vanishing L_x maximises the sensitivity of the horizontal proton position to ξ.

The proton acceptance and measurement accuracy depend critically on the machine optics. While the ultimate optics for lowest t with a $\beta^* = 1540\,\mathrm{m}$ needs a dedicated injection, complicating the commissioning, an intermediate optics with a standard injection might be more easily achievable at the LHC start. We consider an optics with a β^* of $90\,\mathrm{m}$ which can be obtained by unsqueezing the beams after injection.

The basic considerations of this optics are illustrated in Fig. 2. At the Roman Pot position, the deflection of a proton produced in a pp interaction at the IP with transverse coordinates (x_0, y_0), a momentum loss $\xi = \Delta p/p$ and a polar angle $\theta \approx \sqrt{-t}/p$ can be generally expressed by the machine parameters, using the effective length L and the magnification v:

$$x = L_x\,\theta_x + v_x\,x_0 + D\,\xi \tag{1}$$
$$y = L_y\,\theta_y + v_y\,y_0 \tag{2}$$

To push the protons vertically into the acceptance of the forward detectors, the optics was optimised towards a large L_y and $v_y = 0$ (vertical parallel-to-point focussing). With $L_y = 270\,\mathrm{m}$, protons with $-t > 3 \times 10^{-2}\,\mathrm{GeV}^2$ start to be observed in the detectors. The horizontal deflection depends on the momentum loss ξ, the horizontal production angle θ_x, and the transverse coordinate x_0 at the IP. By choosing $L_x = 0$, the emission angle dependence is eliminated. If the vertex coordinate at the IP can be measured with a precision of about $10\,\mu\mathrm{m}$ by the inner tracker of CMS, the momentum loss of diffractive protons can be measured with a precision $\sigma(\xi)$ better than 10^{-3}. In the case of elastically scattered protons, the dependence on the vertex position drops out due to the requirement of collinearity between the two protons.

In summary, the above optics could probably be commissioned at the beginning with not too many complications. It would allow the first measurements of the total cross-section and elastic scattering at low to intermediate t-values. The acceptance for diffractive protons is about $60\,\%$, due to a good acceptance at low t-values, independent of the proton momentum loss.

3 Physics Goals of TOTEM

Without any doubt, a precise measurement of the pp total cross-section σ_{tot} (Fig. 3, left) and of the elastic scattering over a large t-range (Fig. 3, right) is of primary importance in distinguishing between different models of soft proton interactions which exhibit significantly different cross-sections at large energies and large t-values.
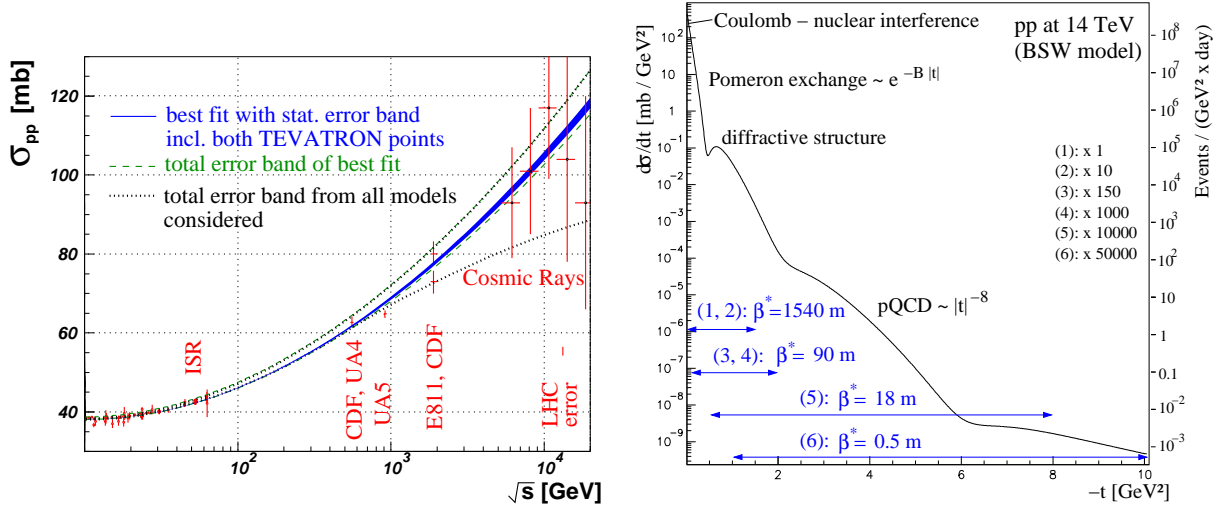

Figure 3: Left: COMPETE fits [7] to all available pp and $p\bar{p}$ scattering data with statistical (blue solid) and total (dashed) error bands, the latter taking into account the Tevatron ambiguity. The outermost curves (dotted) give the total error band from all parameterisations considered. Right: prediction for elastic pp scattering at LHC with one-day statistics for the running scenarios defined in Tab. 1.

3.1 Total Cross-Section

Fig. 3 (left) summarises the existing data from low energies up to collider and cosmic-ray energies. Unfortunately, cosmic-ray data have large uncertainties, and the conflicting data from the TEVATRON demonstrate the difficulty of these measurements and make an extrapolation to higher energies uncertain, leaving a wide range for the expected value of the total cross-section at the LHC energy of $\sqrt{s} = 14\,\mathrm{TeV}$, typically from 90 to 130 mb. Taking into account all available data, the COMPETE collaboration [7] has made an overall fit of the energy dependence of the total cross-section and the ratio ρ of the real to imaginary parts of the elastic scattering amplitude, and predict for the LHC:

$$\sigma_{tot} = 111.5 \pm 1.2^{+4.1}_{-2.1}\,\mathrm{mb}\,, \quad \rho = 0.1361 \pm 0.0015^{+0.0058}_{-0.0025}\,. \tag{3}$$

The precision of the extrapolation is dominated by the ambiguity in the TEVATRON data (second error).

The total pp cross-section is related to the nuclear elastic forward scattering amplitude via the Optical Theorem. This allows a luminosity independent determination based on the total inelastic rate and the extrapolation of the pp elastic scattering to the optical point $t = 0$. Hence a simultaneous measurement of the total inelastic rate and the elastic scattering at the lowest possible $|t|$-values, which requires a large β^*, is needed.

To determine the inelastic rate, TOTEM has made extensive trigger studies that are summarised in Tab. 2. Algorithms have been developed to trigger on charged particles in the two large-acceptance forward telescopes and in the Roman Pot detectors (see Fig. 1, left). Inelastic

Process	σ [mb]	Trigger Losses [mb]		
		Double Arm	Single Arm	After Extrapol.
Minimum bias	58	0.3	0.06	0.06
Single Diffractive	14	–	2.5	0.6
Double Diffraction	7	2.8	0.3	0.1
Double Pomeron	1	–	–	0.02
Elastic Scattering	30	–	–	0.1

Table 2: Trigger losses for double-arm, single-arm and proton trigger (the latter for Double Pomeron Exchange and elastic scattering). In the double-arm trigger at least one particle per hemisphere has to be detected, while in the single-arm only at least one particle in either hemisphere is required.

events are recorded either with a double arm trigger or with a single arm trigger that contains more background mainly from beam-gas events. While most of the non-diffractive events are registered, the largest trigger losses occur in single diffraction. Single diffractive events with masses below $10\,\text{GeV}$ fail the trigger (see the mass acceptance curve in Fig. 7, left), resulting in a trigger loss of $2.5\,\text{mb}$ which, however, can be corrected for, using $\frac{d\sigma}{dM} \propto \frac{1}{M}$. Triggers on just beam crossings will help in the understanding of the trigger algorithms and of the background. The final uncertainties in the inelastic rate are estimated to be around $0.8\,\text{mb}$.
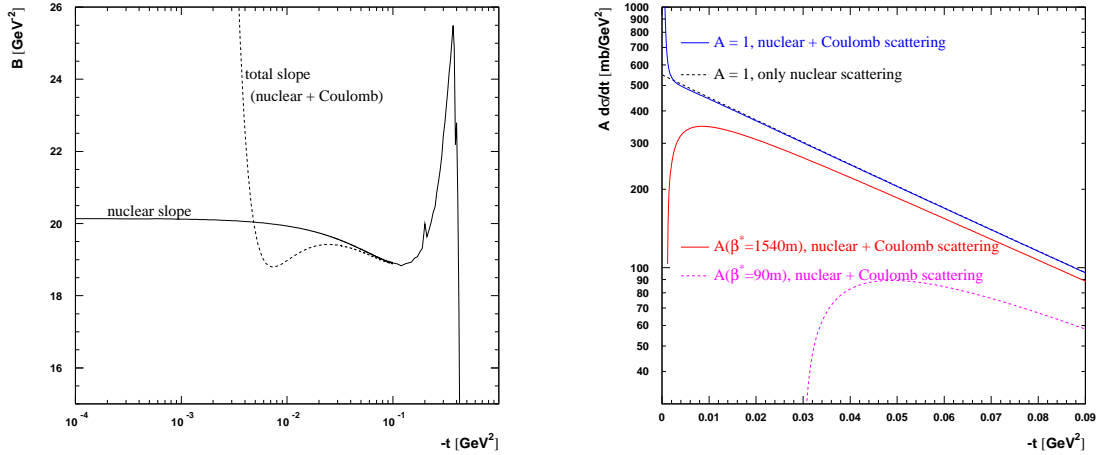

Figure 4: Left: slope parameter $B(t) \equiv -\frac{\frac{d}{dt}\left(\frac{d\sigma}{dt}\right)}{\frac{d\sigma}{dt}}$ of elastic pp scattering with and without Coulomb contribution. Right: differential cross-section of elastic scattering without (top curves) and with (bottom curves) acceptance effect from the Roman Pots at high and intermediate β^*.

The elastic pp scattering with a cross-section of about $30\,\text{mb}$ has to be measured to the lowest possible $|t|$-values to enable an extrapolation to the optical point $t = 0$. The relative statistical uncertainty of the extrapolation is estimated to be $0.1\,\%$ based on 10 hours of data taking with the large β^* optics. Systematic effects, such as the alignment of the detectors with respect to the beams, have to be studied carefully and will probably dominate the error of the extrapolation. Furthermore, this extrapolation is also model dependent due to the way the nuclear–Coulomb interference is treated which influences the exponential slope of the nuclear scattering up to a few $10^{-2}\,\text{GeV}^2$. The slope parameter B of the expected exponential distribution is given in Fig. 4 (left) with and without Coulomb interference. Coulomb effects become negligible for $|t| > 2 \times 10^{-2}\,\text{GeV}^2$. Fig. 4 (right) shows the elastic scattering distribution, also multiplied by the acceptances of the $1540\,\text{m}$ and $90\,\text{m}$ optics. Taking the theoretical uncertainties into account, an ultimate extrapolation precision of about $0.5\,\%$ can be achieved with the highest-β^* optics.

With the acceptance down to $|t| \sim 3 \times 10^{-3} \, \mathrm{GeV}^2$, indications of the Coulomb term will become visible.

It is worth mentioning that, under the assumption of an early commissioning of an optics with $\beta^* = 90 \, \mathrm{m}$, the exponential behaviour of the t-distribution can be measured in the range $0.04 \, \mathrm{GeV}^2 < -t < 0.2 \, \mathrm{GeV}^2$, allowing the determination of the rate at $t = 0$ with a precision better than $5\,\%$. The total cross-section and the luminosity would then be known at early data taking with a similar accuracy. In addition, the transverse vertex distribution at the interaction point ($\sim 0.2 \, \mathrm{mm}$) could be determined with elastic events which would lead to another determination of the luminosity, using the machine parameters:

$$\mathcal{L} = \frac{N^2 \, k \, f}{4 \, \pi \, \sigma_x \, \sigma_y} = \frac{I^2}{4 \, \pi \, f \, k \, \sigma_x \, \sigma_y} \tag{4}$$

3.2 Elastic pp Scattering

Much of the interest in large-impact-parameter collisions centres on elastic scattering and soft inelastic diffraction. High-energy elastic nucleon scattering represents the collision process in which the most precise data over a large energy range have been gathered. The differential cross-section of elastic pp interactions at the LHC, as predicted by the BSW model[8], is given in Fig. 3 (right). Increasing the squared momentum transfer, $-t$, means looking deeper into the proton at smaller distances. Several t-regions with different scattering behaviours can be identified. For $|t| < 10^{-3} \, \mathrm{GeV}^2$, Coulomb scattering ($\propto |t|^2$) is dominant, whereas for $|t| > 10^{-3} \, \mathrm{GeV}^2$, nuclear scattering via Pomeron exchange takes over ($\propto \exp(-B|t|)$), with nuclear-Coulomb interference in between, thus allowing a measurement of the ρ value. At large t-values above $1 \, \mathrm{GeV}^2$, perturbative QCD with e.g. triple-gluon exchange ($\propto |t|^{-8}$) might describe the central elastic collisions of the proton. It is obvious that many different models try to describe the behaviour of the elastic scattering. In particular, the regime of large spacelike $|t|$ is associated with small interquark transverse distances within a proton. Large differences between the models are expected, and hence a high-precision measurement up to $|t| \approx 10 \, \mathrm{GeV}^2$ will help to better understand the structure of the proton.

The elastic scattering distribution extends over 11 orders of magnitude and has therefore to be measured with several different optics scenarios, as described in Tab. 1. Decreasing β^* shifts the observable $|t|$-range to larger values and simultaneously increases the luminosity, compensating the drastic decrease of the cross-section. Even at the largest accepted $|t|$-values ($\sim 10 \, \mathrm{GeV}^2$), limited by the size of the beam tube, about 100 events $/ \, \mathrm{GeV}^2$ are expected for a one-day run. Double Pomeron Exchange will be a substantial background to elastic scattering since the t-distribution is much flatter. A careful check on the collinearity of the two protons is therefore mandatory.

The measurement of the Coulomb/nuclear interference and hence of the ρ parameter is best done when Coulomb and nuclear scattering are of the same order. Demonstrating the possibilities of a rho measurement, Fig. 5 displays the t-value at $50\,\%$ detection efficiency versus the detector distance to the beam for different collider energies. As the closest approach to the beam, 10 times the rms beam spread plus $0.5 \, \mathrm{mm}$ is considered (line with triangles). Thus, at the nominal LHC energy with normal beams, the Coulomb region is not reachable. The almost horizontal line indicates the t-values at which the cross-sections for hadronic and Coulomb scattering are equal. The two ways to approach the Coulomb region are indicated by the arrows. For very low beam intensities and consequently thin beams (low beam emittances), it might be possible to approach the beams closer. A safer way is to reduce the LHC energy. The larger beam spread at lower energies ($\sigma(\theta) \propto s^{-\frac{1}{4}}$) is largely compensated by the lower $|t|$-values at the same emission angle ($-t \approx s \, \theta^2$). Hence a ρ measurement at an energy of $8 \, \mathrm{TeV}$ should be possible.
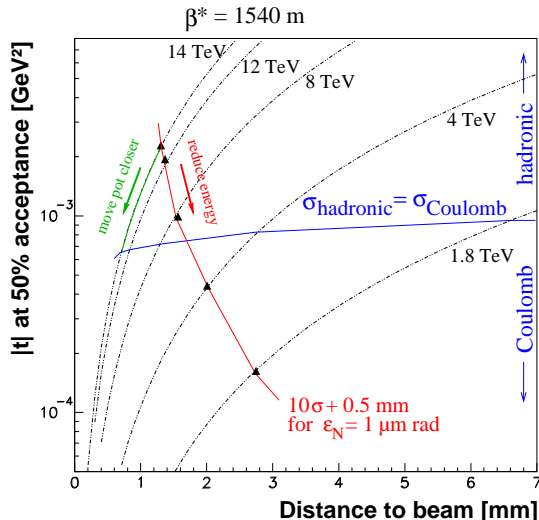
Figure 5: t-value where 50 % acceptance is reached, as a function of the detector distance from the beam centre, for different centre-of-mass energies. The nominal TOTEM operating point is at 14 TeV and a normalised emittance of 1 μm rad implying a detector-beam distance of $10\,\sigma + 0.5\,\mathrm{mm} = 1.3\,\mathrm{mm}$. To access the Coulomb region, either the distance between detector and beam or the energy has to be reduced.

3.3 Diffractive Physics

Most of the soft inelastic diffraction processes via single or double Pomeron exchange (see Fig. 1, right) are peripheral, occurring at collision impact parameters around 1.5 fm. The proton(s) involved may stay intact or dissociate. The events are characterised by the momentum loss ξ, the squared four-momentum transfer t and the azimuthal angle ϕ of the proton and/or by a rapidity gap $\Delta\eta$ which is related to ξ ($\Delta\eta = -\ln\xi$). At the start of the LHC, when the luminosities are low, TOTEM will concentrate on measurements of the individual diffractive cross-sections – single and double diffraction, Double Pomeron Exchange (DPE) – and their dependence on ξ and t. Furthermore, DPE processes leading to low mass final states are an important potential resource for spectroscopy.

With increasing luminosity, semi-hard and hard diffraction – i.e. diffractive processes that contain a hard (short-distance) collision with visible jets in the final state – will come into our reach. The trigger will still be on the forward protons detected in the Roman Pots or on dissociated protons with forward particles in T1 or T2. The basic hard diffractive processes with one or more gaps in the final state are linked together. To really understand these events, one will need to examine the t-distribution of the forward protons for different hardness of the collision process (jet transverse momenta), as well as to study the generalisation to the cases where the proton undergoes soft diffraction. Correlating the jet activities and the jet transverse momenta with the parameters of the forward protons will give a first glance to the understanding of the underlying dynamics. Extraordinarily clean events are those with only two coplanar jets and two unfragmented protons. It is obvious that for these physics a combined CMS/TOTEM detector is needed.

Depending on the running scenarios with different beam foci and luminosities, the acceptances for leading protons change considerably. Fig. 6 (left) shows the (t, ξ) acceptances for low, intermediate and high β^* optics. For $\beta^* = 0.5\,\mathrm{m}$, all protons with $\xi > 2\,\%$ are observed, almost independently of their t-values. For the two other optics, all ξ-values down to 10^{-8} are accepted for $|t| > 2 \times 10^{-3}$ $(3 \times 10^{-2})\,\mathrm{GeV}^2$ for $\beta^* = 1540\,\mathrm{m}$ (90 m). Consequently, a large fraction of the diffractive protons is observed. In particular, the 90 m optics will allow the study of semi-hard and hard diffraction, already at early LHC runs.

Diffractive events are identified in the cleanest possible way by the observation of the forward
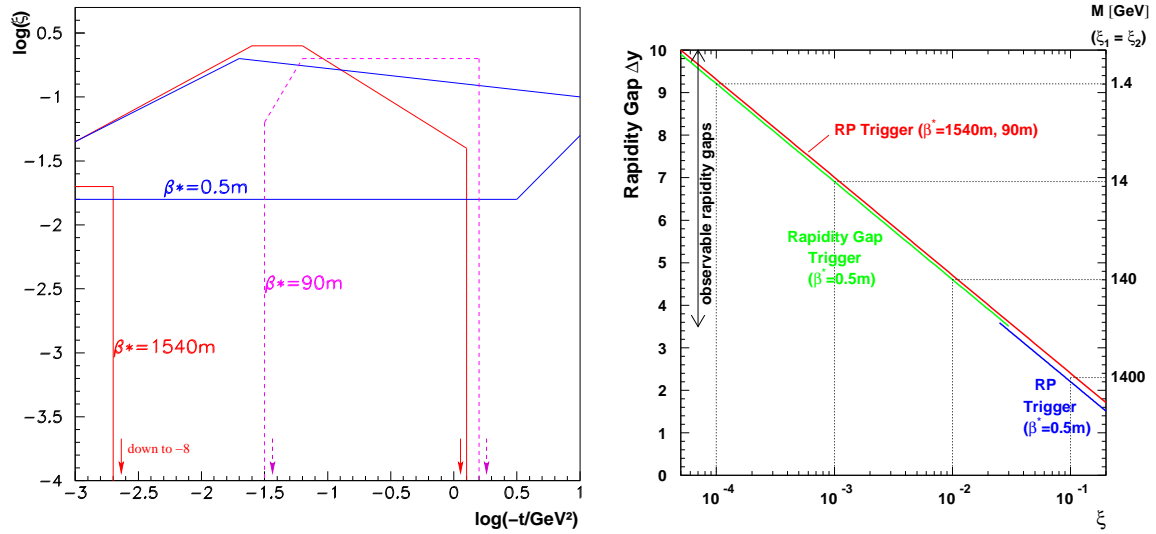
Figure 6: Left: acceptance of the RP station at 220 m for leading protons with squared four-momentum transfer t and momentum loss ξ. For each of the three optics scenarios with $\beta^* = 1540$ m, 90 m and 0.5 m the contour lines of the 50 % acceptance level are drawn. Right: Ranges for triggering DPE events with Roman Pot trigger and rapidity gap trigger for the different optics. Here, the symmetric case of equal momentum loss for the two protons (i.e. $\xi_1 = \xi_2$) is considered.
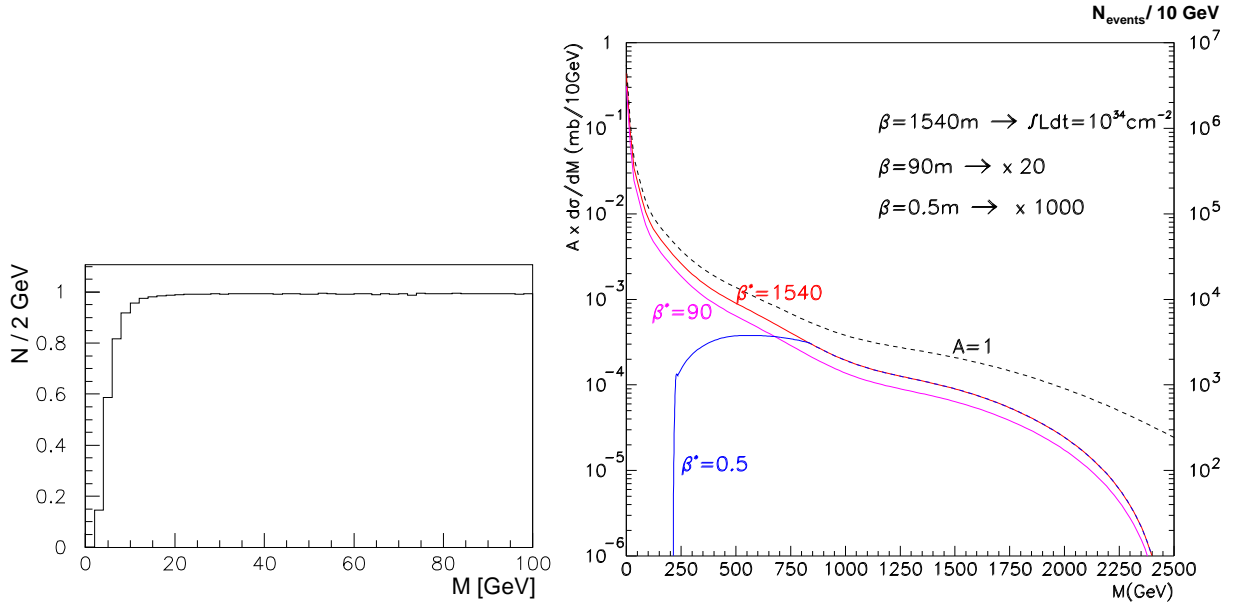

Figure 7: Left: acceptance for Single Diffractive states with mass M using the forward trackers T1 and T2. Right: differential cross-section of Double Pomeron Exchange without (dashed) and with (continuous lines) accounting for the leading-proton acceptance of the Roman Pots for different beam optics.

protons. However, with its large rapidity acceptance in the forward regions, TOTEM can also use the rapidity gap method (measuring the gap between the most forward particle and the proton on the same side) that allows triggering on low ξ values even at $\beta^* = 0.5$ m, thus complementing the direct proton measurement. Fig. 6 (right) shows the ξ acceptance of the Roman Pot trigger and of the rapidity trigger. For $\beta^* = 0.5$ m, the two trigger possibilities are just overlapping thus covering the complete ξ range. How often the rapidity gap survives and is not filled by gluon radiation can be checked with the two other optics scenarios which offer redundancy of

the Roman Pot and rapidity gap triggers. This so-called "rapidity gap survival" is an important quantity when comparing HERA and hadron collider data. Also given on the right-hand scale is the corresponding diffractive mass, produced in DPE for the symmetric case $\xi_1 = \xi_2$.

The DPE mass distribution obtained with a proton trigger on both sides is shown in Fig. 7 (right), also multiplied by the acceptances of the three optics scenarios. With the high and intermediate β^* optics, all masses, down to the lowest values, can be observed, whereas the low β^* optics introduces a mass cut around $250\,\mathrm{GeV}$ but extends the high-mass reach due to the higher luminosity. On the right-hand scale, the number of events for an integrated luminosity of $10^{34}\,\mathrm{cm}^{-2}\,\mathrm{s}^{-1}$ demonstrates that events with masses above $2\,\mathrm{TeV}$ can be observed even with a one-day run at $\beta^* = 1540\,\mathrm{m}$.

The mass acceptance for Single Diffractive states (Fig. 7, left) extends to masses as low as $10\,\mathrm{GeV}$ and hence allows the measurement of the Single Diffractive cross-section without too much extrapolation.

Acknowledgements

References

1. TOTEM: Letter of Intent, CERN-LHCC-97-49, CERN 1997.
2. TOTEM: Technical Design Report, CERN-LHCC-2004-002; addendum CERN-LHCC-2004-020.
3. G. Ruggiero for the TOTEM collaboration: The TOTEM Detectors, this conference.
4. FELIX: Letter of Intent, CERN-LHCC-97-45, CERN 1997.
5. A. Ageev et al. (FELIX Collaboration), J. Phys. G **28**, (2002) R117.
6. R. Engel, Nucl. Phys. B (Proc. Suppl.) **122** (2003) 437-446;
   K. Eggert, ibidem, pp. 447-450.
7. J.R. Cudell et al., PRL **89**, (2002) 201801.
8. C. Bourelly, J. Soffer, T.T. Wu, Eur. Phys. J. **C28**, (2003) 97.